Open Journal of Geology, 2022, 12, 587-612
https://www.scirp.org/journal/ojg
ISSN Online: 2161-7589
ISSN Print: 2161-7570

A Petrological, Geochemical, and Geochronological Study of Shuikou Ultrabasic Rock Mass in Wuding County, Yunnan Province, China

Bin Yang, Zizheng Wang*, Qing Zhou*, Xiaoliang Cui, Shengwei Wang

Chengdu Center, China Geological Survey, Chengdu, China
Email: *15523327@qq.com, *405542917@qq.com

How to cite this paper: Yang, B., Wang, Z.Z., Zhou, Q., Cui, X.L. and Wang, S.W. (2022) A Petrological, Geochemical, and Geochronological Study of Shuikou Ultrabasic Rock Mass in Wuding County, Yunnan Province, China. *Open Journal of Geology*, **12**, 587-612.
https://doi.org/10.4236/ojg.2022.128027

Received: June 13, 2022
Accepted: August 14, 2022
Published: August 17, 2022

Abstract

Geotectonically, the Shuikou ultrabasic-basic rock mass is located on the western margin of the Yangtze Platform. As revealed by field geological surveys, the Shuikou rock mass intrudes into the quartz sandstones of the Sinian Chengjiang Formation (*Zac*). It is dominated by pyroxenites and can be roughly divided into four lithofacies zones, namely gabbros at the outermost periphery and fine-, medium-, and coarse-grained pyroxenites from margin to center. With the transition from pyroxenites to gabbros, the Shuikou rock mass features gradual enrichment in silica and alkali overall, an increase in ΣREE and $(La/Yb)_N$ ratio, and a decrease in δEu values and Eu/Sm ratio, indicating that the Shuikou rock mass was formed from the continuous differentiation and crystallization of consanguineous magma and that low-degree partial melting occurred meanwhile. According to the U-Pb baddeleyite geochronology, the crystallization age of the Shuikou rock mass is 210.7 ± 3 Ma (MSWD = 1.01). Based on this, as well as the analysis of geochemical characteristics, the Shuikou rock mass occurred in a continental intraplate tensional environment, this is closely related to the activities of the Emeishan mantle plume during the same period.

Keywords

Shuikou Rock Mass, Petrological Characteristics, Geochemical Characteristics, Geochronology, Wuding County, Yunnan Province

1. Introduction

Ultrabasic rocks are the products of the activities of stable continental rift zones or deep faults. They originate deeply and are the direct reflection and historical records of deep geodynamic processes in the shallow crust. With the attributes of deep origin and shallow occurrence, the ultrabasic rocks not only bring in important information about the material composition, evolution, tectonics, physics, and chemistry of the deep Earth but are also frequently accompanied by abundant rare earth elements (ERRs) and rare minerals. Therefore, they serve as ideal study objects of petrology, mineral deposit, and geodynamics.

The Emeishan large igneous province (ELIP) exists on the Yangtze Platform. It consists of the "trinity" of rock association including Emeishan basalts, the mafic-ultramafic intrusive rocks widely distributed on the western margin of the Yangtze Plate, and the ultrabasic rocks distributed along the Kangding-Yunnan fault-uplift zone [1]. Among them, the ultrabasic rocks have special significance for the exploration of the genesis of the ELIP as a tracer in geodynamics [2] [3] [4]. Meanwhile, the behavioral characteristics, enrichment, and differentiation of elements in the ultrabasic rocks (*i.e.* the characteristic products in a tensional tectonic environment) may provide reliable information and evidence for the coupling relationships between large-scale magmatic activities in the Emeishan Mountain area and the multiple stages of tensional tectonic evolution in the Kangding-Yunnan fault-uplift zone [5] [6].

The Kangding-Yunnan fault-uplift zone extends from Kangding City, Sichuan Province in the north to Yuanjiang County and Dahongshan Village, Xinping County, Yunnan Province in the south and from the Puduhe and Xiaojiang faults in the east to the Yuanmou-Lvzhijiang fault in the west. It is a narrow and long zone spreading in the NS direction. The part in Yunnan Province of the fault-uplift zone is also called the Kunyang rift. It lies in the Yangtze Block (second-order) of the general Yangtze tectonic zone (first-order) in terms of geotectonic location (**Figure 1(a)**). The Kunyang rift has undergone a long geohistorical evolution since the Early Proterozoic, which contributes to extremely developed structures and magmatic rocks. Meanwhile, the basement structures of the rift are in EW- or NEE-trending and the main structures in the rift are in NS trending [7]. The first-order structures in the rift include parallelling deep faults and the NS-trending boundary faults that control the overall morphology of the rift, the spatial spreading of strata, volcanic activities, and tectonomagmatic metallogenic zones. The second-order structures in the rift were formed from the regional compression in the middle-late developmental stage or closure of the rift. They mainly include SN- and EW-trending faults [8] and are commonly accompanied by fold structures. The second-order faults further complicate the structural pattern of alternating grabens and horsts in the Kunyang rift. As a result, five fault basins were formed in the Huili-Dongchuan and Wuding-Yuanjiang rift troughs, namely Dongchuan, Bijiashan, Wuding, Yimen, and Yuanjiang fault basins. The Shuikou rock mass in this study is located in the Wuding fault basin (**Figure 1(a)**). This time, it is planned to conduct petrological and geochemical research on the Shuikou rock mass, so as to reveal the geological information contained in the Wuding faulted basin during this period and provide basic evidence support for the study of mantle activity in this area.

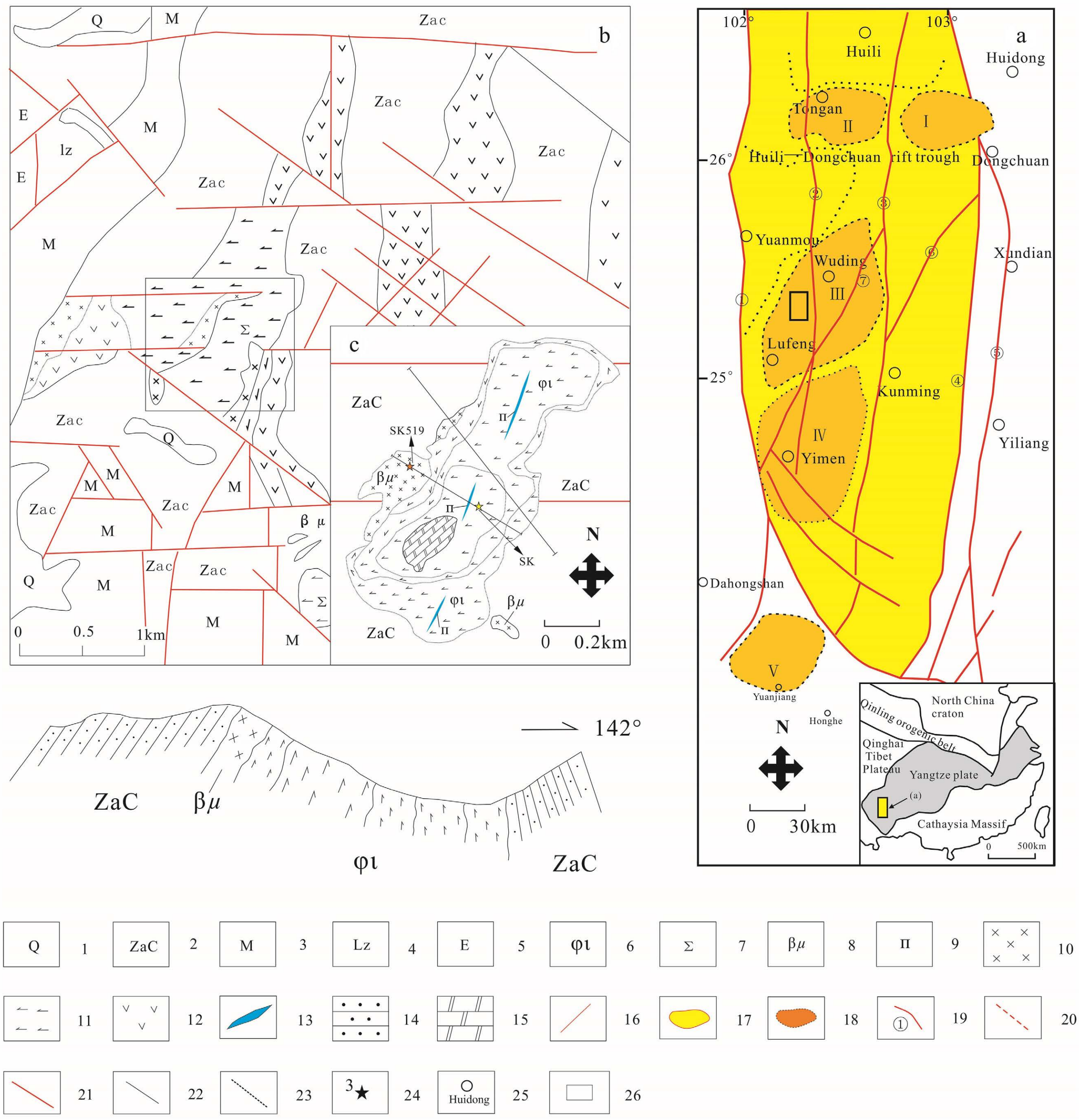

Figure 1. Regional geological map of the Shuikou area, Yunnan Province (a) and the geological map of the Shuikou rock mass (b). 1: The Quaternary; 2: Chengjiang Formation; 3: Late Proterozoic Meidang Formation; 4: Late Proterozoic Lvzhijiang Formation; 5: Mesoproterozoic Etouchang Formation; 6: Pyroxenite; 7: Ultrabasic rock (unclassified); 8: Diabase; 9: Intermediate rock (unclassified); 10: Diabase; 11: Pyroxenite; 12: Andesite; 13: Intermediate dyke; 14: Sandstone; 15: Dolomite; 16: Fault; 17: Southern section of the Panxi rift (Kunyang rift); 18: Fault basin; 19: Deep fault and its no.: ① Yuanmou-Lvzhijiang fault; ② Tanglang-Yimen fault; ③ Puduhe fault; ④ ⑤ Xiaojiang fault; 20: Inferred fault; 21: Measured fault; 22: Geological boundary; 23: Inferred geological boundary; 24: Sampling location; 25: Place name; 26: Scope of the study area.

2. Regional Geology and Rock Mass Geology

Geographically, the Shuikou rock mass is located near the Shuikouqing Reservoir in Bicheng Town, Lufeng County, Yunnan Province (**Figure 1(b)**). It is elliptical in plane, with a long axis in NNE trending, a length of about 1200 m, a width of about 600 m in the middle part, and an area of outcrops of about 1.5 km^2. According to field geological surveys, the Shuikou rock mass develops in the Chengjiang Formation (Zac) and is controlled by the regional Luoci fault. It is distributed in a banded shape in NE trending, with a steep contact attitude and eastward inclination. It mainly occurs in the form of stocks, with no joints developing.

The Shuikou rock mass shows notable magmatic differentiation in plane and distinct lithofacies zones (**Figure 1(c)**). As indicated by petrographic research results (**Figure 2**), the Shuikou rock mass can be divided into four types of rocks according to the grain size of mineral crystals, namely gabbro diabase, and fine-, medium-, and coarse-grained pyroxenites from margin to center. The gabbro diabase constitutes the outermost part of the rock mass. It is grayish-green basic rocks and shows gabbro-diabase texture and blocky structure in the hand specimen in the field. It is gradually transformed into ultrabasic rocks inwards, which can be divided into fine-grained pyroxenites (pyroxene content: 70% - 75%, grain size: 0.12 - 0.25 mm), medium-grained pyroxenites (pyroxene content: 85% - 90%, grain size 0.7 - 2 mm), and coarse-grained pyroxenites (pyroxene content: 90%, grain size: 1.2 - 2.5 mm, the maximum grain size: 4.5 mm; **Figure 2(f)**) inward according to the grain size of mineral crystals. The hand specimens of the pyroxenites are dark gray and slightly green and exhibit pyroxene texture and dense blocky texture in the field (**Figure 2(e)**). Meanwhile, the pyroxenites mostly show inequigranular texture or granular mosaic texture (hornblende inlaid with pyroxene) under a microscope. The grain size of pyroxenes in the hand specimens of coarse- and medium-grained pyroxenites can reach 2 - 5 cm and 1 - 2 cm, respectively.

Despite the chronological controversy, it has been roughly determined that the Shuikou rock mass was formed during the Late Hercynian-Indosinian [9]-[12] and slightly later than the Emeishan basalts [13].

A greyish-white intermediate dyke (**Figure 2(c)**, **Figure 2(d)**) is visible in the coarse-grained pyroxenes. It is 1 - 30 cm wide and shows distinct and straight boundaries. Meanwhile, it extends for 3 - 10 m toward the two ends and disappears in the medium- and fine-grained pyroxenes.

The Shuikou rock mass shows the following lithologic changes from center to margin. In terms of main minerals, pyroxenes reduce from 90% to 30% - 70%, olivine reduces from 25% to a low content or even disappears, and hornblendes are gradually replaced by biotite. In contrast, the plagioclase content is zero in the center but is up to greater than 70% on the margin. These types of rocks in the Shuikou rock mass are distributed in a stratoid form, with distinct boundaries and different mineral composition and structural characteristics. Overall,

Figure 2. Geological and petrographic study of the Shuikou rock mass. (a) Diagram of the zoning of the Shuikou rock mass (zones from northwest to southeast: sandstones of the Chengjiang Formation → coarse-grained pyroxenites → medium-grained pyroxenites → fine-grained pyroxenites → diabase); (b) Boundary between medium- and coarse-grained pyroxenites (strongly weathered); (c) Intermediate dyke Π crossing coarse-grained pyroxenites (width: 13 - 18 cm); (d) Intermediate dike Π crossing medium-grained pyroxenites (width: 20 - 40 cm); (e) Residual carbonatite (κc) mixed in coarse-gained pyroxenites; (f) Comparison of hand specimens of coarse-, medium-, and fine-grained pyroxenites; (g) Hand specimen of diabase at the periphery of the Shuikou rock mass; (h), (i) Photos of coarse-grained pyroxenites under a microscope (Carlsbad twinning or polysynthetic twinning are formed in pyroxenes, magnetite scatters and vein-like aggregates are distributed around pyroxenes, and plagioclase bears polysynthetic twinning, with a grain size 0.5 - 1.3 mm. Hornblende is brown, with weak polychromaticity, a grain size 0.7 - 2 mm, and two sets of measured cleavage of (110) ∧ (100) = 86˚±); (j) Photo of medium-grained pyroxenites under a microscope (twinning is rarely formed in pyroxenes, and large numbers of magnetite particles with intact crystal forms fill between pyroxene grains); (k) Fine-grained pyroxenites (feldspar and hornblende significantly increase, and most of them underwent alternation. Therefore, it is difficult to find pyroxene grains with intact crystal forms); (l), (m) Photos of diabase under a microscope (typical gabbro texture has been formed, pyroxenes are lowly intact due to alteration, feldspars are elongated, and it is difficult to observe twinning).

the Shuikou rock mass shows distinct zones, big lithologic changes, and wide marginal facies zones. Meanwhile, it clearly evolved from ultrabasic rocks in the center to the basic rocks on the margin, which is closely related to magmatic differentiation.

3. Collection and Analysis of Samples

Samples were collected in two stages according to the results of the field geological survey and petrographic study. At the first stage, the core in the southern part of the Shuikou rock mass was sampled along the predetermined section lines in the SE-NW direction of 330˚ (**Figure 1(c)**). A total of 13 samples were collected at this stage. They covered coarse-grained and medium-grained pyroxenites and were set as the "SK" series. At the second stage, the northwestern margin of the Shuikou rock mass was sampled along the predetermined section lines in the SE-NW direction of 330˚ (**Figure 1(c)**). A total of 12 samples were collected at this stage. They covered fine-grained pyroxenites and diabase and were set as the SK519 series. All the samples were collected from representative fresh outcrops. They were peeled indoors, broken to about 2 cm × 2 cm pieces, and then crushed to powders of less than 200 meshes for chemical analysis. Both major and trace elements (including rare earth elements) in the samples were measured at the National Geological Experiment and Testing Center, China Geological Survey. The major element analysis was carried out using an X-ray fluorescence spectrometer (PW4400) according to the method described in standard GB/T14506.28-2010. The analyses of trace elements and rare earth elements (REEs) were conducted using a plasma mass spectrometer (X-series) according to the method stated in standard DZ/T0223-2001.

LA-ICP-MS U-Pb isotopic dating was conducted on the baddeleyite mainly selected from the samples of fine-grained pyroxenites and diabase. The rock crushing, baddeleyite selection, target preparation, and cathodoluminescence (CL) images were completed in Beijing GeoAnalysis Co., Ltd. and the LA-ICP-MS zircon U-Pb isotopic dating was carried out at the LA-ICP-MS laboratory in the School of Marine Sciences, Sun Yat-sen University, Guangzhou Province. The software ICPMS-DataCal was employed to process the experiment data, and the program Isoplot/Ex_ver3 was used to plot the concordia diagrams of the U-Pb isotope data and calculate the weighted average ages of the samples.

4. Geochemical Characteristics

4.1. Characteristics of Major Elements

The major element analysis results of the Shuikou rock mass are shown in **Table 1**. As shown in this table, the major elements of the SK-series samples are as follows. The SiO_2 content is 41.95% - 43.83%, with an average of 43.1%, and thus the SK-series samples are ultrabasic. Meanwhile, the samples have a TiO_2 content of 1.33% - 2.39%, (average: 1.72%), a Al_2O_3 content of 5.46% - 9.66% (average:

Table 1. Analytical and calculation results of major elements in the Shuikou ultrabasic-basic rocks (wt%).

Sample No.		SiO_2	TiO_2	Al_2O_3	Fe_2O_3	FeO	MnO	MgO	CaO	Na_2O	K_2O	P_2O_5	LOI	SI*	$Mg^{\#*}$	m/f*	AR*
SK1	Coarse-grained pyroxenite	43.18	1.94	13.03	4.91	6.77	0.19	8.57	13.78	4.51	1.15	0.27	0.59	33.07	0.69	1.35	1.54
SK2	Coarse-grained pyroxenite	43.65	2.09	8.21	5.65	6.27	0.16	12.21	17.58	1.98	0.41	0.18	0.41	40.04	0.78	1.90	1.20
SK3	Coarse-grained pyroxenite	43.38	2.39	7.67	6.35	6.63	0.17	11.77	18.31	1.46	0.28	0.09	0.78	44.43	0.76	1.69	1.14
SK4	Coarse-grained pyroxenite	43.83	1.65	9.66	4.92	6.81	0.17	11.04	18.06	1.84	0.36	0.18	0.42	44.21	0.74	1.73	1.17
SK5	Medium-grained pyroxenite	41.82	1.83	8.13	7.97	7.49	0.2	13.15	17.4	0.85	0.1	0.08	0.15	44.48	0.76	1.59	1.08
SK6	Coarse-grained pyroxenite	43.71	1.73	9.24	6.74	6.59	0.2	11.25	16.52	2.04	0.42	0.2	0.39	41.60	0.75	1.57	1.21
SK7	Coarse-grained pyroxenite	44.06	1.37	11.41	4.62	5.77	0.17	10.72	16.39	2.75	0.42	0.13	1.51	44.15	0.77	1.90	1.26
SK8	Coarse-grained pyroxenite	43.2	1.33	12.4	7.4	4.38	0.19	9.75	14.27	4.66	0.92	0.41	0.57	35.96	0.80	1.56	1.53
SK9	Medium-grained pyroxenite	41.95	0.86	3.84	4.22	10.6	0.28	22.72	12.01	0.44	0.04	0.04	1.39	39.75	0.79	2.79	1.06
SK10	Medium-grained pyroxenite	44.79	1.46	8.48	3.98	6.31	0.17	13.95	16.38	2.16	0.44	0.16	0.89	31.97	0.80	2.50	1.23
SK11	Medium-grained pyroxenite	34.22	2.72	5.46	12.9	13.22	0.3	17.31	11.05	0.59	0.09	0.07	0.06	39.24	0.70	1.25	1.09
SK12	Medium-grained pyroxenite	42.59	1.41	7.65	4.57	8.48	0.21	16.61	13.82	2.03	0.42	0.12	0.59	31.72	0.78	2.34	1.26
SK13	Medium-grained pyroxenite	42.88	1.99	10.06	5.5	6.77	0.19	11.16	16.04	2.34	0.57	0.25	0.97	42.36	0.75	1.68	1.25
SK519-1	Fine-grained pyroxenite	46.16	3.81	13.51	6.52	7.6	0.23	5.53	7.51	4.33	0.53	0.79	2.32	22.56	0.56	0.72	1.60
SK519-2	Fine-grained pyroxenite	46.52	3.76	13.65	6.59	7.6	0.23	5.48	7.29	4.3	0.63	0.71	2.29	22.27	0.56	0.71	1.62
SK519-3	Fine-grained pyroxenite	45.99	3.65	13.77	6.66	7.28	0.22	5.35	7.27	4.22	0.7	0.72	2.47	22.09	0.57	0.71	1.61
SK519-4	Fine-grained pyroxenite	45.3	3.83	13.68	6.19	7.99	0.24	5.63	8.01	3.87	0.69	0.74	2.43	23.1	0.56	0.73	1.53
SK519-5	Fine-grained pyroxenite	45.19	3.88	13.8	6.57	7.71	0.24	5.68	8.3	3.78	0.7	0.74	2.51	23.24	0.57	0.73	1.51

Continued

SK519-6	Fine-grained pyroxenite	46.26	3.97	13.28	6.93	6.74	0.22	5.14	7.78	4.51	0.66	0.75	2.53	21.43	0.58	0.70	1.65
SK519-7	Diabase	45.59	3.69	14.02	6.99	6.95	0.23	5.38	8.28	4	0.52	0.74	2.6	22.56	0.58	0.72	1.51
SK519-8	Diabase	46.31	3.69	14.12	6.88	6.84	0.22	5.23	7.31	4.17	0.88	0.73	2.4	21.79	0.58	0.71	1.62
SK519-9	Diabase	45.93	3.66	13.71	6.12	7.71	0.24	5.47	7.93	3.85	0.93	0.65	2.41	22.71	0.56	0.73	1.57
SK519-10	Diabase	46.55	3.68	14.33	6.84	6.52	0.22	4.62	7.9	4.36	0.7	0.77	2.62	20.05	0.56	0.64	1.59
SK519-11	Diabase	46.22	3.75	13.66	6.83	7.24	0.23	5.38	7.34	4.32	0.6	0.77	2.36	22.07	0.57	0.71	1.61
SK519-12	Diabase	45.43	3.65	13.89	6.59	7.38	0.23	5.21	7.91	3.98	0.68	0.72	2.75	21.85	0.56	0.69	1.54

Note: tested in: National Geological Experiment and Testing Center, China Geological Survey; testing instrument: X-ray fluorescence spectrometer (PW4400); testing method: XRF method; testing data: October 2019; Note: SK series: pyroxenite samples; SK519 series: gabbro samples; Note: SK series: ultrabasic pyroxenite samples; SK519 series: basic pyroxenite samples. Consolidation index SI = 100 × MgO/(MgO + FeO + Fe_2O_3 + Na_2O + K_2O) (wt%); Fe/Mg ratio m/f = (Mg^{2+} + Ni^{2+})/(Fe^{2+} + Fe^{3+}Mn) (atomic ratio); Magnesium index $M^{\#}$= Mg^{2+}/(Mg^{2+} + Fe^{2+}) (atomic ratio); Alkalinity ratio AR = AI_2O_3 + CaO + (Na_2O + K_2O)/AI_2O_3 + CaO-(Na_2O + K_2O) (wt%).

8.06%), a Fe_2O_3 content of 4.22% - 7.97% (average: 5.73%), a MgO content of 9.75% - 13.95% (average: 13.42%), a CaO content of 12.01% - 17.58% (average: 15.5%), a Na_2O content of 0.85% - 4.51%, a K_2O content of 0.04% - 1.15%), a K_2O + Na_2O content of 1.74% - 3.17% (average: 2.12%), a Na_2O/K_2O ratio of 3.92 - 8.5, and a MnO content of 0.17% - 0.28%. The loss on ignition (LOI) of the samples is 0.15% - 0.59%. The ultrabasic pyroxenites have a low LOI (0.15% - 0.97%), which is consistent with the absence of hydrothermal alteration in the rocks observed under a microscope. Additionally, the samples have a Mg/Fe ratio of m/f = 1.35 - 2.5, a solidification index of SI = 39.24 - 51.97, an alkalinity ratio of AR = 1.06 - 1.25, and a magnesium index of $Mg^{\#}$ = 0.69 - 0.80.

The major element analysis results of the SK519-series samples are as follows. The SiO_2 content is 45.3% - 46.52%, with an average of 46.007%, and thus the SK519-series are basic rocks. Specially, for samples SK519-1 - SK519-6 that were considered fine-grained pyroxenites in the field survey, their chemical analysis results of major elements show that their SiO_2 content has reached the standard of basic rocks. Therefore, samples SK519-1 - SK519-6 are considered basic rock samples in data analysis but were still defined as fine-grained pyroxenites in petrographic analysis and field sampling. The SK519-series samples have a TiO_2 content of 3.65% - 3.88% (average: 3.73%), a Al_2O_3 content of 13.51% - 14.12% (average: 13.78%), a Fe_2O_3 content of 6.12% - 6.99% (average: 6.73%), a MgO content of 4.62% - 5.68% (average: 5.34%), a CaO content of 7.27% - 8.3% (average: 8.44%), a Na_2O content of 3.85% - 4.51%, a K_2O content of 0.52% - 0.93%, a K_2O + Na_2O content of 4.48% - 5.17% (average: 4.82%), and a Na_2O/K_2O ratio of 5.6 - 8.1. The LOI of the SK519-series samples is 2.32% - 2.75%. The basic gabbros have a high LOI (2.32% - 2.75%), which may be related to the intense sub-amphibolization and chloritization of pyroxenes in the basic gabbros observed under a microscope. Additionally, the SK519-series samples have a Mg/Fe ratio of m/f = 0.64 - 0.73, a solidification index of SI = 22.07 - 23.1, an alkalinity ratio of AR = 1.51 - 1.62, and a magnesium index of $Mg^{\#}$ = 0.56 - 0.58.

On the total alkali vs. silica (TAS) diagram of the Shuikou rock mass (**Figure 3**), all ultrabasic pyroxenite samples fall in the picrite basalt zone except for one sample, which falls within the alkaline basalt zone. In comparison, the basic gabbro samples mainly fall in the basalt and trachybasalt zones. All basic gabbro samples and most pyroxene samples fall above the Ir boundary, thus belonging to the alkaline series. Two pyroxene samples fall on the Ir boundary and thus belong to the sub-alkaline-alkaline series. Meanwhile, three pyroxene samples fall below the Ir boundary and thus belong to the sub-alkaline series. For them, it is necessary to further determine whether they are tholeiite or calc-alkaline series. Therefore, a SiO_2-FeO/MgO diagram was plotted (**Figure 4**), in which all the three samples fall in the tholeiite zone and thus are tholeiites.

In the SiO_2-Alk diagram of the Shuikou ultrabasic-basic rock mass (**Figure 5**), all basic gabbro samples and most pyroxenite samples fall in the zone of alkaline series and only two pyroxenite samples fall in the zone of tholeiite series, which is consistent with the TAS diagram and SiO_2-FeO/MgO diagram.

Overall, the gabbros and most pyroxenites in the Shuikou rock mass belong to the alkaline series, and a small number of pyroxenites belong to the tholeiite series. From the ultrabasic pyroxenites to the basic gabbros, the rock mass experience a gradual transition from sub-alkaline tholeiite series to alkaline series.

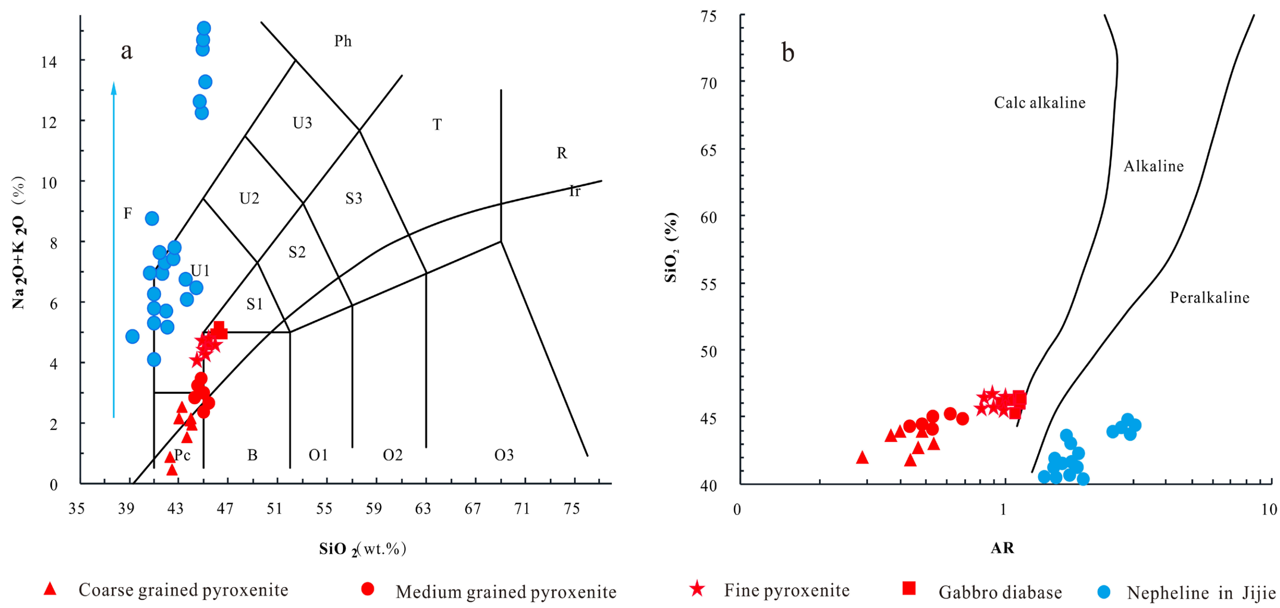

Figure 3. TAS diagram of the Shuikou ultrabasic-basic rock mass (after [14] for the base map). Pc: picrite basalt; B: basalt; O1: basaltic andesite; O2: andesite; O3: dacite; R: rhyolite; S1: trachybasalt; S2: basaltic trachyandesite; S3: trachyandesite; T: trachyte and trachydacite; F: feldspathoidite; U1: tephrite and basanite; U2: phonolitic tephrite; U3: tephritic phonolite; Ph: phonolite; Ir: Irvine boundary, the parts above and the part below Ir are alkaline and sub-alkaline, respectively (after [15]).

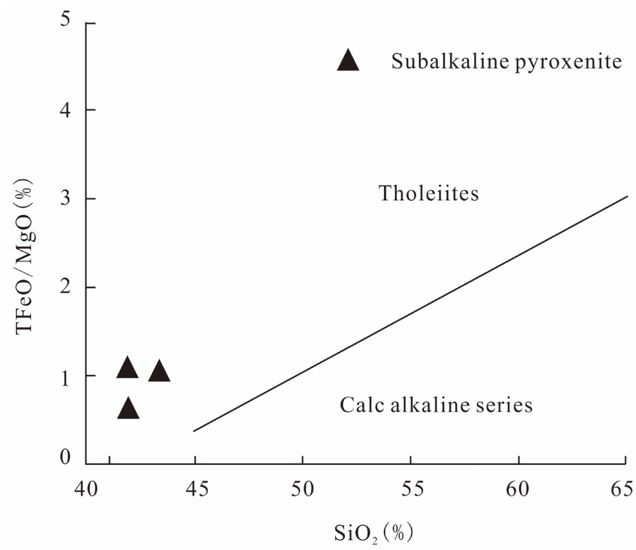

Figure 4. SiO_2-FeO/MgO diagram of the sub-alkaline pyroxenite of the Shuikou rock mass (after [16] for the base map).

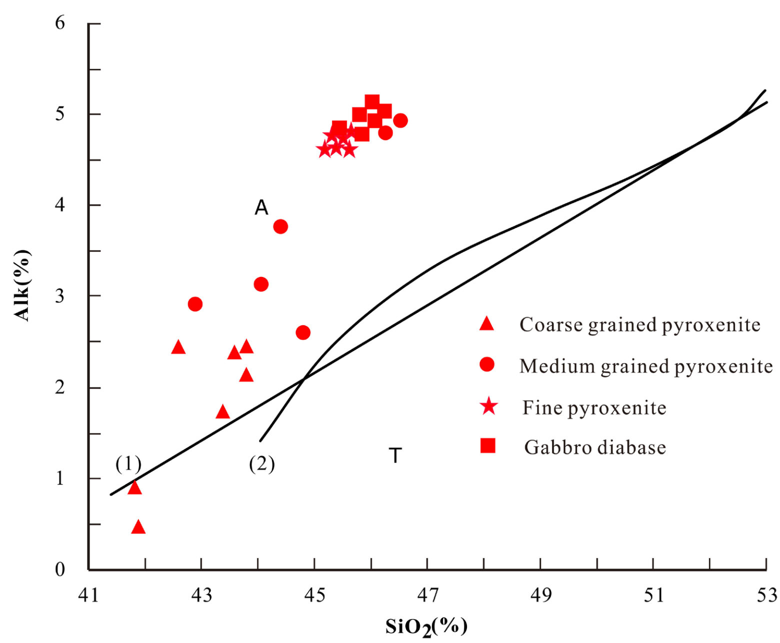

Figure 5. SiO_2-Alk diagram of the Shuikou ultrabasic-basic rock mass (after [17] for the base map). Alk = Na_2O + K_2O; The boundary of the basalt series in Hawaii; 2: the boundary of basalt series around the world; A: alkaline basalt series; T: tholeiite series.

According to the calc-alkaline index diagram of the Shuikou rock mass (**Figure 6**), the calc-alkaline index CA is about 47.2 (<51), indicating that the rock mass belongs to the alkaline series. As shown in the Na_2O-K_2O diagram of the rock mass (**Figure 7**), all gabbro samples fall in the zone of sodium series except for two ones, which fall into the zone of potassium series. In contrast, all pyroxenite samples fall in the zone of the sodium series.

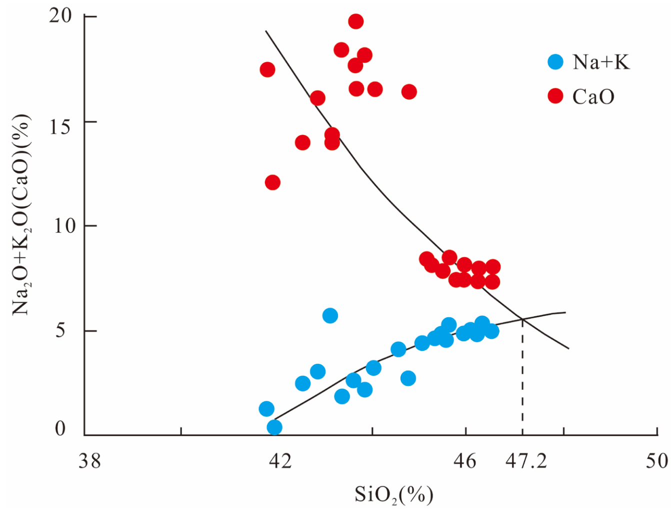

Figure 6. Calculation diagram of calc-alkaline index (CA) of the Shuikou rock mass.

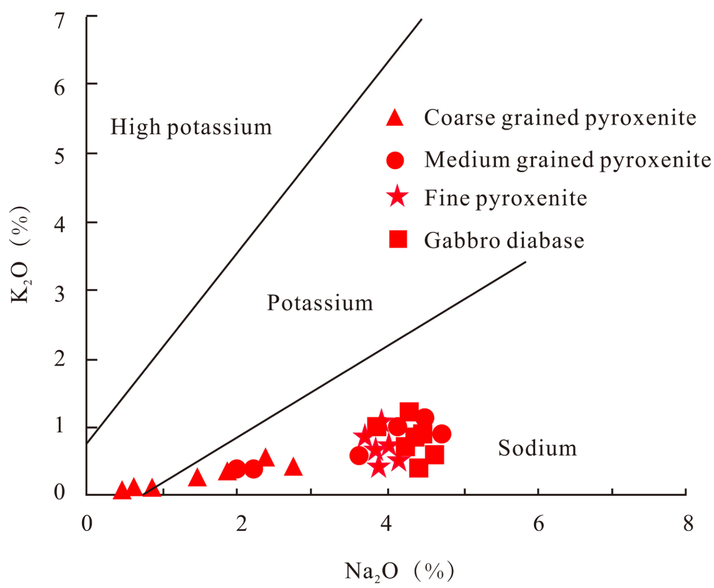

Figure 7. K_2O-Na_2O diagram of the Shuikou rock mass (after [18] for the base map).

According to the TiO_2-MgO diagram of the Shuikou rock mass (**Figure 8**), all the gabbro samples fall in the zone of high-titanium basalts. Meanwhile, all pyroxenite samples also fall in the zone of high-titanium basalts except for three ones, which fall in the zone of low-titanium basalts. These are consistent with the high-titanium characteristics of Emeishan basalts, indicating the affinity between the sources of the two types of rocks.

4.2. Trace Elements

The trace element analysis results of the ultrabasic pyroxenite samples of the Shuikou rock mass are shown in **Table 2**. The ultrabasic SK-series samples have

Table 2. (a) Analytical results of trace elements and rare earth elements of SK-series samples of the Shuikou ultrabasic pyroxenes (10^{-6}); (b) Results of trace elements and rare earth element analyses of SK519-series samples of the Shuikou basic gabbros (10^{-6}).

(a)

Sample No.	SK1	SK2	SK3	SK4	SK5	SK6	SK7	SK8	SK9	SK10	SK11	SK12	SK13
	Coarse-grained pyroxenite	Coarse-grained pyroxenite	Coarse-grained pyroxenite	Coarse-grained pyroxenite	Medium-grained pyroxenite	Coarse-grained pyroxenite	Coarse-grained pyroxenite	Coarse-grained pyroxenite	Medium-grained pyroxenite	Medium-grained pyroxenite	Medium-grained pyroxenite	Medium-grained pyroxenite	Medium-grained pyroxenite
La	3.36	3.55	3.94	4.06	2.07	5.92	3.11	7.41	1.41	6.47	2.41	4.85	3.92
Ce	7.74	7.89	9.65	9.79	5.76	13.6	8.69	15.8	3.74	13.6	5.91	10.1	8.92
Pr	1.25	1.20	1.55	1.56	1.06	1.99	1.54	2.25	0.63	1.88	0.91	1.48	1.50
Nd	6.36	6.27	8.18	7.83	5.52	9.39	7.81	10.2	3.16	8.58	4.36	6.50	7.51
Sm	1.95	1.84	2.40	2.32	1.83	2.56	2.36	2.69	0.99	2.24	1.26	1.73	2.24
Eu	0.94	0.89	1.06	1.02	0.80	1.11	0.97	1.10	0.45	0.86	0.57	0.71	1.03
Gd	2.54	2.58	3.12	3.00	2.51	3.29	3.01	3.10	1.41	2.80	1.68	2.10	2.98
Tb	0.41	0.38	0.48	0.49	0.38	0.50	0.49	0.51	0.21	0.43	0.24	0.33	0.45
Dy	2.50	2.22	2.87	2.85	2.41	3.03	2.97	3.04	1.34	2.45	1.40	2.01	2.82
Er	1.26	1.10	1.38	1.41	1.17	1.51	1.45	1.54	0.61	1.21	0.70	0.99	1.44
Tm	0.19	0.16	0.20	0.20	0.18	0.21	0.19	0.21	0.09	0.16	0.10	0.14	0.19
Yb	1.16	1.01	1.29	1.21	1.05	1.42	1.31	1.36	0.58	1.04	0.65	0.83	1.32
Lu	0.18	0.14	0.19	0.18	0.15	0.18	0.17	0.20	0.09	0.15	0.09	0.11	0.18
Y	11.8	10.2	12.9	12.9	11.1	14.0	13.1	13.8	5.64	11.2	6.32	8.84	13.0
Rb	13.6	5.76	5.74	5.52	2.67	6.93	5.91	11.4	1.70	8.06	2.55	6.92	8.97
Sr	410	233	242	233	135	275	242	399	57.8	281	102	209	258
Ba	130	78.1	116	85.0	32.7	105	51.6	128	16.2	86.7	28.0	66.2	73.3
Ga	15.9	13.6	15.1	15.7	16.9	15.4	13.5	15.5	6.98	12.2	18.7	11.5	13.7
Nb	8.73	6.87	7.51	6.64	2.40	8.38	3.71	8.87	0.97	8.50	3.33	6.63	6.36
Ta	0.60	0.52	0.55	0.49	0.25	0.58	0.32	0.58	0.13	0.57	0.36	0.50	0.45
Zr	41.2	41.6	57.3	54.8	41.0	61.0	57.3	55.8	20.0	49.8	27.9	37.7	47.1
Hf	1.68	1.87	2.45	2.20	1.74	2.24	2.12	1.86	1.05	1.97	1.19	1.59	2.14
Th	0.33	0.27	0.42	0.39	0.19	0.58	0.26	0.56	0.14	0.57	0.17	0.38	0.36
V	372	390	432	376	460	342	299	233	158	328	734	303	357
Cr	123	404	385	174	363	331	171	135	945	693	1081	891	68.0
Co	52.0	57.4	58.6	57.9	79.4	63.3	52.9	54.6	124	59.0	134	79.6	59.7
Ni	64.0	102	120	82.0	137	103	77.5	78.7	322	218	369	303	75.6
U	0.07	0.05	0.08	0.08	0.05	0.14	0.06	0.12	0.05	0.11	0.05	0.07	0.07
Nb/Ta	14.55	13.21	13.65	13.55	9.60	14.45	11.59	15.29	7.46	14.91	9.25	13.26	14.13
Zr/Hf	24.52	22.25	23.39	24.91	23.56	27.23	27.03	30.00	19.05	25.28	23.45	23.71	22.01
Th/U	4.71	5.40	5.25	4.88	3.80	4.14	4.33	4.67	2.80	5.18	3.40	5.43	5.14
Ba/Nb	14.89	11.37	15.45	12.80	13.63	12.53	13.91	14.43	16.70	10.20	8.41	9.98	11.53
Nb/Yb	7.53	6.80	5.82	5.49	2.29	5.90	2.83	6.52	1.67	8.17	5.12	7.99	4.82
Th/Yb	0.28	0.27	0.33	0.32	0.18	0.41	0.20	0.41	0.24	0.55	0.26	0.46	0.27
Sm/Nd	0.31	0.29	0.29	0.30	0.33	0.27	0.30	0.26	0.31	0.26	0.29	0.27	0.30
Eu/Nd	0.15	0.14	0.13	0.13	0.14	0.12	0.12	0.11	0.14	0.10	0.13	0.11	0.14

(b)

Sample No.	SK519-1	SK519-2	SK519-3	SK519-4	SK519-5	SK519-6	SK519-7	SK519-8	SK519-9	SK519-10	SK519-11	SK519-12
	Fine-grained pyroxenite	Fine-grained pyroxenite	Fine-grained pyroxenite	Fine-grained pyroxenite	Fine-grained pyroxenite	Fine-grained pyroxenite	Diabase	Diabase	Diabase	Diabase	Diabase	Diabase
La	17.3	17.0	17.4	16.4	16.5	16.5	15.5	17.0	16.0	16.2	16.3	18.0
Ce	48.7	47.3	48.5	46.2	46.2	46.2	44.0	47.5	44.5	43.8	45.8	47.0
Pr	7.60	7.46	7.51	7.16	7.11	7.20	6.82	7.28	6.80	6.91	7.16	7.53
Nd	39.1	39.3	37.8	36.9	37.1	37.5	36.0	38.0	34.8	35.8	37.5	39.5
Sm	11.0	11.2	10.9	10.3	10.2	10.5	10.0	10.5	9.70	10.3	10.4	11.0
Eu	3.50	3.56	3.51	3.33	3.42	3.25	3.33	3.45	3.18	3.18	3.37	3.70
Gd	13.2	13.4	13.2	12.5	12.5	12.6	12.0	12.8	12.3	12.3	12.9	14.0
Tb	2.10	2.17	2.02	1.93	1.91	1.98	1.90	2.00	1.81	1.87	2.01	2.13
Dy	12.5	13.0	11.9	11.7	11.6	12.0	11.6	12.1	11.4	11.6	12.1	13.0
Er	7.57	7.93	7.46	7.15	7.10	7.44	6.94	7.48	7.00	6.91	7.47	7.77
Tm	0.97	1.02	0.96	0.92	0.91	0.95	0.86	0.98	0.90	0.89	0.96	0.97
Yb	6.42	6.46	6.37	5.83	5.98	6.17	5.92	6.33	5.76	5.76	6.23	6.23
Lu	0.95	1.00	0.96	0.91	0.87	0.92	0.86	0.94	0.88	0.84	0.93	0.93
Y	71.5	78.1	71.0	66.0	66.8	68.0	63.8	71.4	66.7	68.1	70.3	80.1
Rb	7.66	10.0	10.8	10.1	10.2	9.61	6.88	13.6	13.3	9.43	8.48	8.12
Sr	611	670	757	781	790	543	710	852	799	576	619	913
Ba	598	768	863	992	1006	594	609	1361	1575	607	597	766
Ga	22.0	22.6	22.9	22.1	23.3	20.9	21.5	23.0	22.0	22.5	22.4	23.4
Ta	0.88	0.88	0.86	0.83	0.79	0.84	0.75	0.84	0.80	0.76	0.83	0.82
Zr	393	402	388	349	347	362	323	387	381	333	365	356
Hf	8.44	8.44	8.30	7.54	7.61	8.07	7.18	8.35	7.83	7.29	7.94	7.91
Th	1.47	1.50	1.48	1.32	1.28	1.40	1.24	1.46	1.39	1.25	1.41	1.44
V	351	354	348	387	388	379	354	358	362	351	339	324
Cr	127	132	127	129	131	120	112	140	135	97.9	117	123
Co	41.7	41.1	42.0	45.5	45.5	42.4	41.6	42.5	43.6	40.0	42.9	39.8
Ni	36.3	36.3	37.9	39.9	40.6	43.0	36.2	45.8	39.6	33.7	37.3	36.6
U	0.40	0.40	0.38	0.36	0.34	0.38	0.34	0.49	0.37	0.34	0.38	0.36
Nb/Ta	15.11	15.45	15.58	15.06	15.57	15.00	15.33	15.60	15.25	15.26	15.18	15.12
Zr/Hf	46.56	47.63	46.75	46.29	45.60	44.86	44.99	46.35	48.66	45.68	45.97	45.01
Th/U	3.68	3.75	3.89	3.67	3.76	3.68	3.65	2.98	3.76	3.68	3.71	4.00
Ba/Nb	44.96	56.47	64.40	79.36	81.79	47.14	52.96	103.89	129.10	52.33	47.38	61.77
Nb/Yb	2.07	2.11	2.10	2.14	2.06	2.04	1.94	2.07	2.12	2.01	2.02	1.99
Th/Yb	0.23	0.23	0.23	0.23	0.21	0.23	0.21	0.23	0.24	0.22	0.23	0.23
Sm/Nd	0.28	0.28	0.29	0.28	0.27	0.28	0.28	0.28	0.28	0.29	0.28	0.28
Eu/Nd	0.09	0.09	0.09	0.09	0.09	0.09	0.09	0.09	0.09	0.09	0.09	0.09

Note: tested in: National Geological Experiment and Testing Center, China Geological Survey; testing instrument: plasma mass spectrometer (X-series); testing method: mass spectrometry; testing date: October 2019.

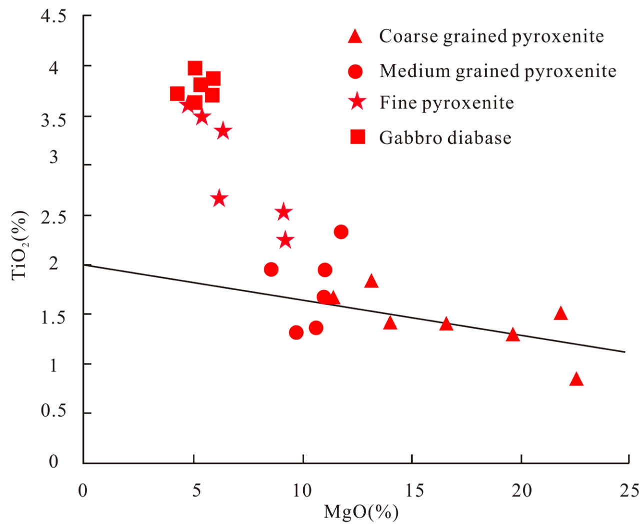

Figure 8. TiO_2-MgO diagram of the Shuikou rock mass (after [19] for the base map).

a Rb content of 2.55 × $10^{−6}$ - 13.6 × $10^{−6}$, a Ba content of 16.2 × $10^{−6}$ - 130 × $10^{−6}$, a Sr content of 57.8 × $10^{−6}$ - 410 × $10^{−6}$, a Nb content of 3.33 × $10^{−6}$ - 13.3 × $10^{−6}$, a Ta content of 0.25 × $10^{−6}$ - 0.6 × $10^{−6}$, a Zr content of 20 × $10^{−6}$ - 61 × $10^{−6}$, a Hf content of 1.05 × $10^{−6}$ - 2.14 × $10^{−6}$, a Th content of 0.14 × $10^{−6}$ - 0.58 × $10^{−6}$, a U content of 0.05 × $10^{−6}$ - 0.12 × $10^{−6}$, and a La content of 2.07 × $10^{−6}$ - 7.41 × $10^{−6}$.

Table 2 also shows the trace elements in the basic rocks (SK519 series) of the Shuikou rock mass. The basic rock samples have a Rb element of $7.66^{−6}$ - 10.8 × $10^{−6}$, a Ba content of 598 × $10^{−6}$ - 1975 × $10^{−56}$, a Sr content of 611 × $10^{−6}$ - 913 × $10^{−6}$, a Nb content of 11.5 × $10^{−6}$ - 13.6 × $10^{−6}$, a Ta content of 0.75 × $10^{−6}$ - 0.88 × $10^{−6}$, a Zr content of 323 × $10^{−6}$ - 402 × $10^{−6}$, a Hf content of 7.18 × $10^{−6}$ - 8.44 × $10^{−6}$, a Th content of 1.24 × $10^{−6}$ - 1.5 × $10^{−6}$, a U content of 0.34 × $10^{−6}$ - 0.4 × $10^{−6}$, and a La content of 15.5 × $10^{−6}$ - 18 × $10^{−6}$. Among them, the contents of K, Ba, Sr, Zr, Rb, and Nb are obviously higher than those of the primitive mantle [20], implying that the primitive magma of the basic rocks in the Shuikou rock mass originated from the low-degree partial melting of the mantle.

According to the spider diagram of primitive mantle-normalized trace elements (Figure 9), the ultrabasic and basic rocks in the Shuikou rock mass show roughly the same distribution pattern of trace elements. In detail, they show obvious hump-shaped curves, with relatively positive anomalies of large-ion lithophile elements (LILEs) such as K, Ba, and Sr (especially Ba) and no notable anomalies of high field strength elements (HFSEs) such as Nb, Ta, Zr, and Hf. This distribution pattern is similar to the trace element curves of basalts from continental rifts but is notably different from the distribution pattern of trace elements in the basic rocks in an island arc environment, which shows strong depletion in HFSEs such as Nb, Ta, Zr, and Hf [22]. Meanwhile, it is closer to the distribution pattern of trace elements in ocean island basalts (OIB) and Emeishan high-titanium basalts. LILEs are extremely liable to enter fluid facies and

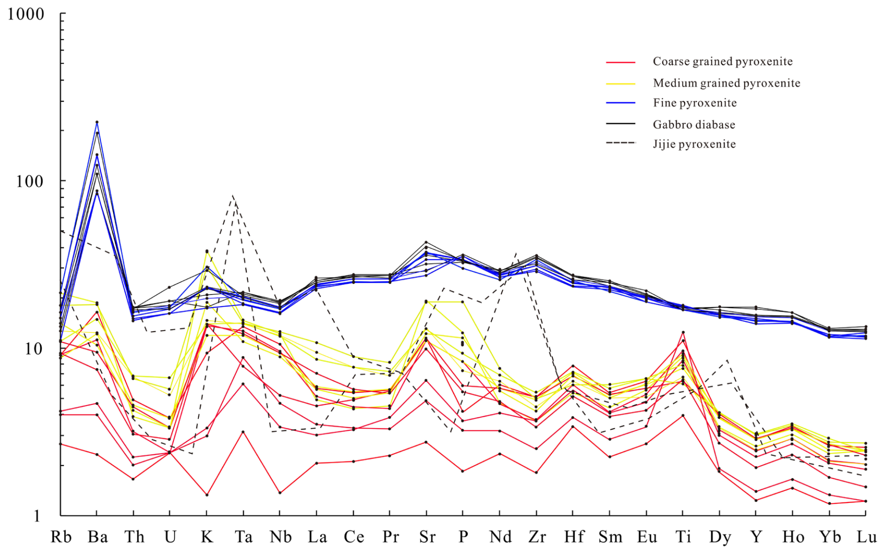

Figure 9. Spider diagram of primitive mantle-normalized trace elements of the Shuikou rock mass (after [21] for normalized data).

migrate during the partial melting of the mantle. Moreover, the lower the melting degree of the mantle in the evolution of mantle magma, the more notable the enrichment in LILEs. Therefore, the enrichment in LILEs of the Shuikou rock mass may indicate the low melting degree during the evolution of mantle magma. Meanwhile, the ultrabasic rocks show more notable enrichment in LILEs than the basal rocks, indicating that the primitive mantle-derived magma of the pyroxenites has a lower degree of partial melting. Additionally, the ultrabasic rocks show more notable enrichment in Ti than the basic rocks, which may indicate that the magma in the ultrabasic rocks features stronger ilmenite differentiation in the early magmatic evolution.

Overall, the contents of various trace elements in the diabase at the periphery are significantly higher than those in pyroxenites and they change as follows from the ultrabasic pyroxenites to the basic gabbros. The Rb and Ba gradually rich and Th shows consistent depletion characteristics. The contents of La, Ce, and Pr notably increase but do not show distinct enrichment and depletion characteristics. Sr shows consistent enrichment characteristics in these types of rocks. Zr is depleted in the ultrabasic rocks but enriched in the diabase. Hf is enriched in the ultrabasic rocks but slightly depleted in the diabase. Ti is notably enriched in the ultrabasic rocks but shows no distinct enrichment and depletion characteristics in the diabase. Y is notably depleted in the ultrabasic rocks but shows no distinct enrichment and depletion characteristics in the diabase. The contents of Ba, Sr, and Zr significantly increase, while the contents of other elements slightly change. The Nb/Ta ratio slightly varies. It is 7.46 - 15.29 for the ultramafic rocks and 15 - 15.58 for the basic rocks, indicating that the two types of rocks experienced significant Nb-Ta fractionation and possess the characteristics of mantle-derived rocks. The Zr/Hf ratio increases. It is 19.05 - 30 for the ultrabasic rocks and 44.86 - 47.63 for the basic rocks, both of which approach the

Zr/Hf ratio of the primitive mantle (36.06). The Th/U ratio slightly changes. It is 2.8 - 5.43 for the ultrabasic rocks and 2.98 - 4 for the basic rocks, both of which approach the Th/U ratio of the primitive mantle (4.05). The Ba/Nb ratio increases from the ultrabasic pyroxenites to the basic gabbros and is 8.41 - 15.45 and 44.96 - 129.1, respectively, which are higher than the Ba/Nb ratio of crustal rocks. This reflects the characteristics of lithospheric mantle, indicating that the Shuikou rock mass possesses mantle-derived magma. The Ta/Hf ratio decreases from the ultrabasic pyroxenites to the basic gabbros and is 0.9 - 2.6 and 0.7 - 0.82 respectively, both of which are greater than 0.3. This might indicate that, similar to the Emeishan basalts, the primitive basaltic magma of the Shuikou rock mass is also derived from a mantle plume [23].

Table 2 shows the characteristic values of REEs of ultrabasic-basic rock samples of the Shuikou rock mass. For the ultrabasic pyroxenites (SK series) in the study area, the total REE (ΣREE) content is 20.59×10^{-6} - 63.78×10^{-6}, the total light rare earth element (ΣLREE) content is 10.38×10^{-6} - 26.78×10^{-6}, and the total heavy rare earth element (ΣHREE) content is 11.45×10^{-6} - 24.72×10^{-6}. Therefore, the ΣREE content is low and the ΣLREE/ΣHREE ratio is 0.88 - 1.69, indicating no distinct fractionation between the LREEs and the HREEs. Meanwhile, the $(La/Yb)_N$ ratio of the ultrabasic pyroxenites is 1.70 - 4.46, with an average of 2.64. The δEu values of the ultrabasic pyroxenites are 1.1 - 1.29, with an average of 1.18, indicating slight positive anomalies of Eu. The δCe values are 0.23 - 0.86 (average: 0.6) for all the SK-series samples, except sample SK13, of which the δCe value is 1.35, indicating negative Ce anomalies. Additionally, Eu/Sm = 0.38 - 0.48 and Sm/Nd = 0.26 - 0.33 for the SK-series samples. Overall, the total ΣREE content of the ultrabasic rocks is low and widely varies, and there is no distinct fractionation between LREEs and HREEs of the ultrabasic rocks.

For the basic gabbros (SK519 series), the ΣREE content is 221.86×10^{-6} - 254.54×10^{-6}, the ΣLREE content is 114.98×10^{-6} - 127.20×10^{-6}, and the ΣHREE content is 106.21×10^{-6} - 125.752×10^{-6}. Therefore, the ΣLREE/ΣHREE ratio is 0.99 - 1.1. The $(La/Yb)_N$ ratio of the basic gabbros is 1.88 - 2.07, with an average of 2.64. The δEu values of the basic gabbros are 0.86 - 0.93, with an average of 0.91, indicating weak negative anomalies of Eu. The δCe values of the basic gabbros are 0.28 - 2.45, with an average of 0.7. Additionally, Eu/Sm = 0.30 - 0.33 and Sm/Nd = 0.27 - 0.29 for the basic gabbros. Overall, the total ΣREE content in the basic rocks is high and varies in a small range, and there is no distinct fractionation between LREEs and HREEs of the basic rocks.

From ultrabasic to basic rocks, the δEu values, Sm/Nd ratio, and Eu/Sm ratio decrease, while the ΣREE content and $(La/Yb)_N$ ratio increase. This indicates that the Shuikou rock mass was formed from the successive differentiation and crystallization of consanguineous magma, which is consistent with the changing pattern of the main elements.

As shown in the spider diagram of chondrite-normalized REE patterns of the Shuikou rock mass in **Figure 10**, both the ultrabasic and basic gabbros are present

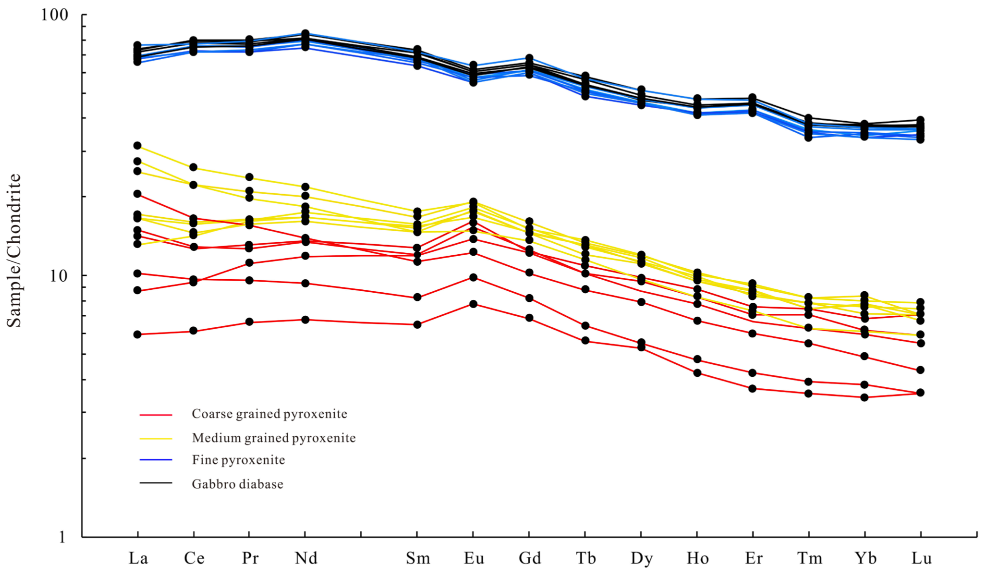

Figure 10. Spider diagram of chondrite-normalized REE patterns of the Shuikou rock mass (after [26]).

as rightward curves with high left and low right overall. The curves are gentle and very similar, suggesting that both types of rocks should be the products of mantle-derived magmas. Meanwhile, the overall chondrite-normalized REE patterns are similar to those of Emeishan basalts and OIB [24]. The basic gabbros show weak negative anomalies of Eu and Ce, reflecting that a certain amount of plagioclase has crystallized and precipitated from parental magmas. Plagioclase is rich in Ca^{2+}, which can be replaced by Eu^{2+} to form isomorphism and the magma may originate from the melting of deep parts [25]. The ultrabasic pyroxenes show weak positive anomalies of EU, reflecting that no plagioclase has crystallized and precipitated from parental magmas. Sr is a strongly compatible element in plagioclase, and Eu may replace Sr^{2+} in the plagioclase in the form of equivalent Eu^{2+}, thus leading to the enrichment of Eu.

5. U-Pb Baddeleyite Dating

Baddeleyite sample 020AH was dated in this study. A total of 17 points were analyzed and relevant data are shown in **Table 3**. According to the cathodoluminescence (CL) images of baddeleyite in **Figure 11**, most baddeleyite grains are hypidiomorphic short columnar, granular, or broken in shape, with a length of 60 - 100 um. As shown in the U-Pb concordia diagram of baddeleyite from the ore-bearing gabbros of the Shuikou rock mass (**Figure 12**), the 17 points of sample 020AH are evenly distributed around the concordant curve, with a degree of concordance of roughly higher than 90%. The $^{206}Pb/^{238}U$ ages of the 17 points vary in the range of 180 - 220 Ma. In the U-Pb baddeleyite weighted age diagram of the Shuikou rock mass (**Figure 12**), the weighted average age is 210.7 ± 3 Ma (MSWD = 1.01), which is roughly consistent with the U-Pb zircon age (204 Ma) obtained by Zou [27] within the error range. This can reflect that the

Shuikou rock mass was crystallized during the Late Triassic Indosinian and at the peak (258 - 208 Ma) of the strong tensile fracture of the Panxi rift.

Table 3. U-Pb baddeleyite dating data of gabbros of the Shuikou rock mass.

Point no.	$^{207}Pb/^{235}U$	2σ	$^{206}Pb/^{238}U$	2σ	rho	Age$^{207}Pb/^{235}U$	2σ	Age$^{206}Pb/^{238}U$	2σ	Disc.
020AH13.D	0.288	0.014	0.0344	0.0010	0.3515	257 Ma	11.0	218.1 Ma	6.5	15.14
021AH14.D	0.289	0.017	0.0340	0.0014	0.0246	258 Ma	13.0	215.3 Ma	8.5	16.55
022AH15.D	0.383	0.037	0.0346	0.0031	0.9302	329 Ma	27.0	219.0 Ma	19.0	33.43
023AH16.D	0.250	0.022	0.0352	0.0013	0.5571	226 Ma	18.0	223.1 Ma	7.9	1.28
024AH17.D	0.253	0.008	0.0330	0.0007	0.6159	229 Ma	6.6	209.4 Ma	4.5	8.36
025AH18.D	0.240	0.017	0.0324	0.0026	0.8061	218 Ma	14.0	205.0 Ma	16.0	5.96
027AH19.D	0.288	0.044	0.0317	0.0025	0.7648	256 Ma	35.0	201.0 Ma	16.0	21.48
028AH20.D	0.315	0.019	0.0333	0.0013	0.8332	278 Ma	14.0	211.5 Ma	7.9	23.92
029AH21.D	0.241	0.010	0.0334	0.0010	0.0278	219 Ma	8.4	211.5 Ma	6.0	3.47
030AH22.D	0.292	0.015	0.0336	0.0008	0.1015	260 Ma	12.0	213.3 Ma	4.7	17.96
031AH23.D	0.246	0.023	0.0316	0.0015	0.0231	223 Ma	18.0	200.5 Ma	9.2	10.09
032AH24.D	0.258	0.023	0.0320	0.0014	0.7214	232 Ma	18.0	202.8 Ma	8.5	12.59
035AH25.D	0.235	0.012	0.0328	0.0009	0.3015	214 Ma	9.7	208.2 Ma	5.3	2.89
037AH27.D	0.268	0.018	0.0342	0.0007	0.3505	241 Ma	14.0	216.9 Ma	4.1	10.00
038AH28.D	0.260	0.017	0.0344	0.0014	0.1134	235 Ma	14.0	217.8 Ma	8.4	7.32
039AH29.D	0.346	0.052	0.0337	0.0026	0.9693	301 Ma	39.0	214.0 Ma	16.0	28.90
040AH30.D	0.243	0.009	0.0319	0.0006	0.4663	221 Ma	7.3	202.2 Ma	3.6	8.34

Note: tested in: LA-ICP-MS laboratory in the School of Marine Sciences, Sun Yat-sen University; testing instrument: Agilent 7700e; testing method: LA-ICP-MS; testing date: August 2019.

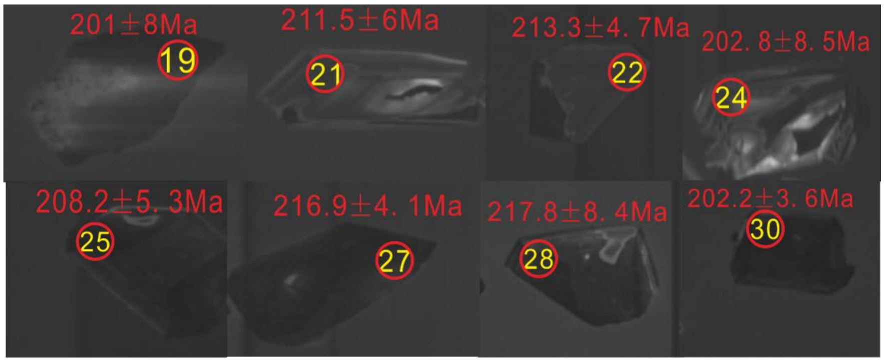

Figure 11. Representative CL images of the baddeleyite from the ore-bearing gabbros of the Shuikou rock mass. **Note:** circles denote testing positions, nos. in the circles corresponds to test nos., and age values represent $^{238}U/^{206}Pb$ epigenetic ages.

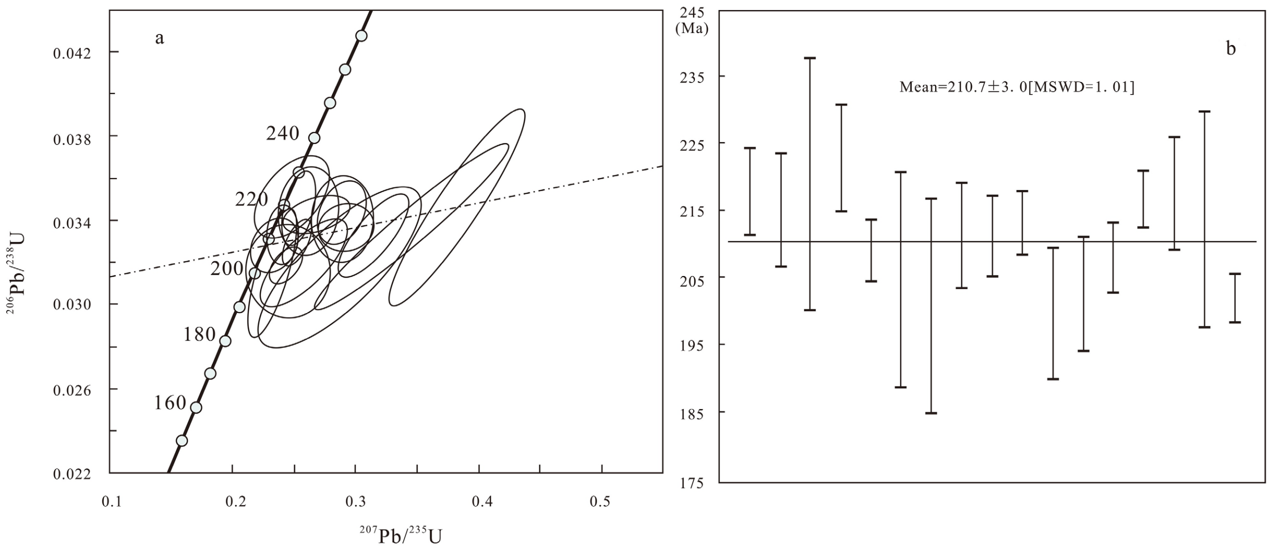

Figure 12. Concordia diagram of U-Pb baddeleyite ages and U-Pb weighted age diagram of baddeleyite of the Shuikou rock mass.

6. Questions and Discussion

6.1. Properties and Evolutionary Characteristics of Magma Sources

According to the above-mentioned geochemical characteristics of major elements, the Shuikou rock mass is rich in Ca, Na, AI, and Ti, and depleted in Mg and K. From the ultrabasic rocks toward the basic rocks, the contents of Al_2O_3, Na_2O, and K_2O and alkalinity ratio AR of the rock mass increase, and thus the rock mass are gradually rich in silica and alkali in general. In comparison, the contents of MgO, CaO, and FeO, Fe/Mg ratio m/f, and the consolidation index SI decrease from the ultrabasic rocks toward the basic rocks. The magnesium index $Mg^{\#}$ of the ultrabasic pyroxenites is 0.69 - 0.80 (average: 0.77), which is higher than that of primitive magma (0.68 - 0.75 [28]). The Mg# of the basic gabbros varies in a small range of 0.56 - 0.58, which is lower than that of primitive magma. In the (Me + Fe)/K-Si/K correlation diagram of the Shuikou rock mass (**Figure 13**), all the pyroxenite and gabbro samples fall on a line after fitting, which may imply that the two types of rocks in the Shuikou rock mass were formed from the gradual differentiation and crystallization of consanguineous magma [29].

As shown in the diagrams of the correlation between the MgO and various major elements of the Shuikou rock mass (**Figure 13**), there is a strong linear correlation between MgO and various major elements [30] [31]. This indicates that the rock mass was formed from the continuous evolution of primitive magma and that the evolution was dominated by magmatic crystallization and differentiation. In detail, MgO is negatively correlated with SiO_2, $A1_2O_3$, TiO_2, and K_2O + Na_2O, and is positively correlated with FeO, indicating that the primitive magma of the Shuikou rock mass was formed from the evolution of mantle-derived

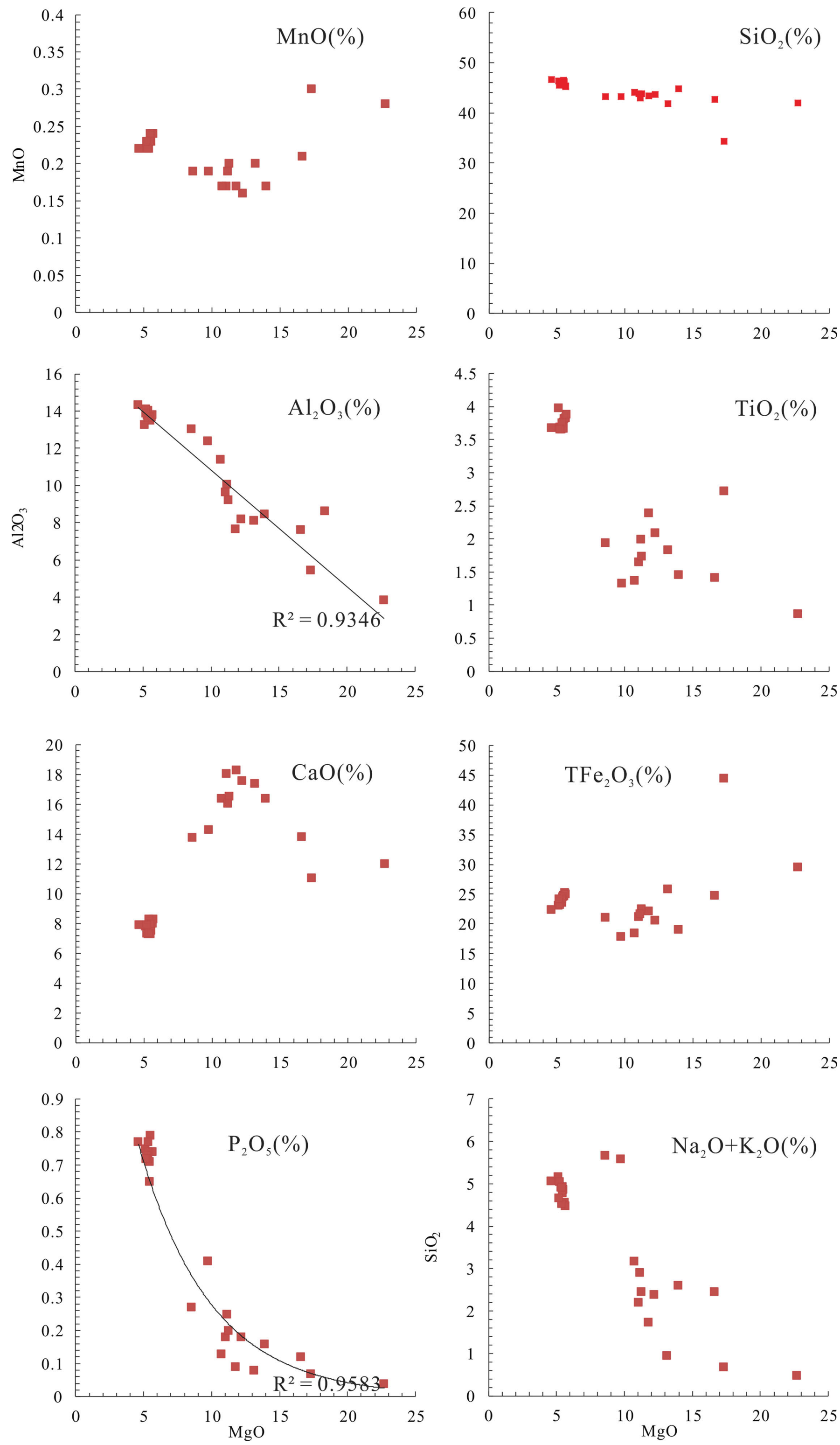

Figure 13. Diagrams of the correlation between MgO and major elements (%) in the Shuikou rock mass.

magma. The reason is that SiO_2, $A1_2O_3$, TiO_2, K_2O, and Na_2O are all compatible components and FeO is an incompatible component during the mantle melting.

Moreover, MgO is nearly linearly correlated with $A1_2O_3$, TiO_2, and P_2O_5. Since $A1_2O_3$ and TiO_2 mainly occur in magnetite and ilmenite and P_2O_5 mainly occur in apatite, the linear correlation between MgO and them indicates that a small number of paragenetic minerals such as magnetite, ilmenite, and apatite crystallized with the differentiation of magma, which is consistent with the observation results of the rock mass under a microscope. Additionally, MgO is first positively and then negatively correlated with CaO. In the early stage of the magmatic evolution, CaO mainly occurred in pyroxenes. Then MgO was negatively correlated with CaO when MgO > 12%, indicating that the primitive magma in the pyroxenites underwent separation and crystallization of rocks dominated by pyroxenes [32]. The correlation between MgO and MnO is not distinct and the MnO content is stable.

The trace elements are discussed as follows. According to the La-La/Sm diagram of the Shuikou rock mass (**Figure 14**), the rock mass shows high La-Sm differentiation, the pyroxene samples are distributed in the form of an oblique line, and the basic gabbro samples are distributed in the form of a horizontal line. As can be inferred from this as well as the characteristics of major elements, the magmatic evolution of the Shuikou rock mass experienced both partial melting and crystallization and differentiation. However, the partial melting mainly occurred inside the gabbro at the beginning of the formation of the ultrabasic rocks, while the crystallization and differentiation are dominant throughout the diagenism of the rock mass [33] [34].

6.2. Tectonic Environment

In petrological studies, the results of the geodynamic environment of ancient rocks will be controversial if they are inferred from geochemical indicators. Nevertheless, this method is still widely applied [36]. The reason is as follows. If the studied rocks were formed in a modern tectonic environment, their element associations and relevant geochemical parameter ratios are relatively consistent. In this case, the tectonic environment at the time of rock formation can be obtained through inverse using a series of suitable geochemical diagrams [37]. Therefore, this study explores the tectonic setting of the Shuikou rock mass using the diagrams that can be used to effectively discriminate the formation environment of basalts, as well as the characteristics of contemporary diabase on the western margin of the Yangtze Platform.

Geotectonically, the Shuikou rock mass is located in the Wuding fault basin in the Kangding-Yunnan fault-uplift zone on the western margin of the Yangtze Platform. According to the stratigraphic contact relationships in the field, the magmatic activities in the study area are closely related to the multi-stage magmatic activities in the tensional environment during the Hercynian-Indosinian period in the Kangding-Yunnan fault-uplift zone [20], which is related to activities of the Emeishan mantle plume. As a "probe" in the study of a tectonic environment, trace elements in magmatic rocks are of low contents and stable

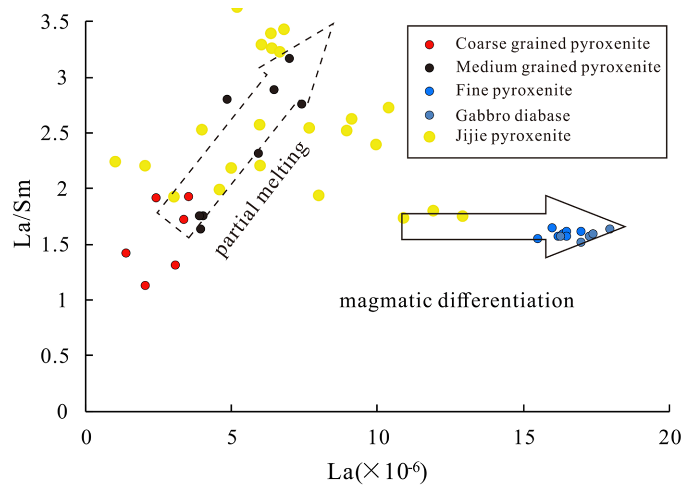

Figure 14. La-La/Sm diagram of the Shuikou rock mass (after [35]).

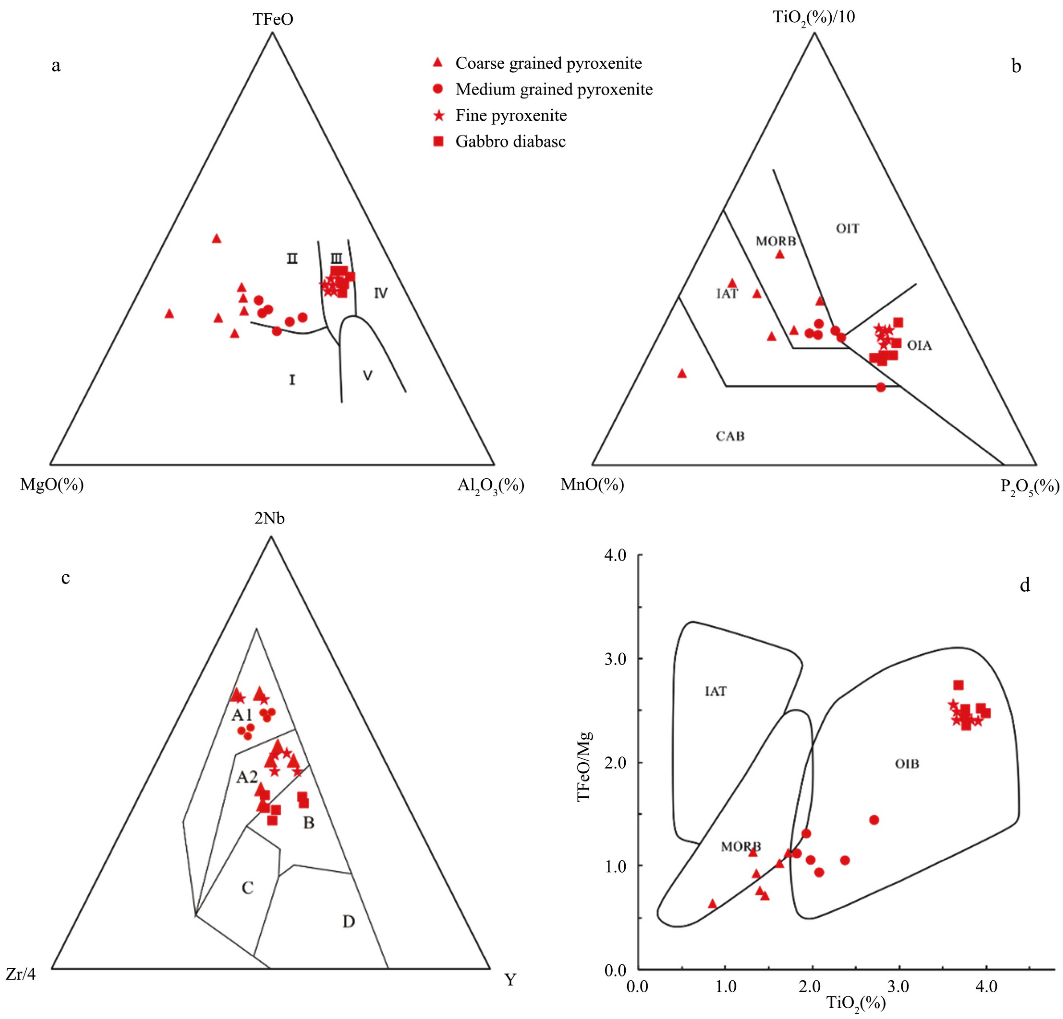

Figure 15. A-T-K discrimination diagram and Nb-Zr-Y discrimination diagram of the tectonic setting of the Shuikou rock mass. (a): I: Oceanic basalts; II: Continental basalts; III: Basalts of isl-and arcs ad orogenic belts; (b), (c), (d): A1 + A2: intraplate alkaline basalts; A2 + C: intraplate tholeiite; B: P-type MORB; D: N-type MORB; C + D: volcanic arc basalt.

and are not liable to be affected by the contamination of lithospheric components [21]. Therefore, they relatively correspond to geological activities and can accurately reflect the initial tectonic environment of the rock mass. Inactive elements such as Nb, Zr, and Y remain stable during magmatic evolution and can be used to judge the tectonic setting of a rock mass [24]. As shown in the Nb-Zr-Y diagram (**Figure 15**), all the rock samples fall in the continental intraplate alkaline basalt zone except for several gabbro samples, which fall in the continental intraplate tholeiite zone. As shown in the A-T-K discrimination diagram of the tectonic environment (**Figure 15**), all the rock samples fall in the continental basalt zone except for two samples, which fall in the oceanic basalt zone [38]. Therefore, the Shuikou rock mass mainly shows an intraplate tectonic setting that is similar to that of the OIB, and thus it should be formed in a continental intraplate tensile environment.

7. Conclusions

1) The study of petrology and petrography shows that the main lithology of the Shuikou rock body is pyroxenite, and the rock body can be roughly divided into four lithofacies zones from the edge to the center of the rock body: gabbro and diabase are at the periphery, and fine-grained medium-grained coarse-grained pyroxenite is, in turn, transited to the interior.

2) The gabbros and most pyroxenites in the Shuikou rock mass belong to the alkaline series, and a small number of pyroxenites belong to the tholeiite series. From the ultrabasic pyroxenites to the basic gabbros, the rock mass experience a gradual transition from sub-alkaline tholeiite series to alkaline series. As indicated by the geochemical characteristics of the rocks, the Shuikou rock mass was possibly formed from the gradual differentiation and crystallization of homologous magma and the magmatic evolution was dominated by crystallization and differentiation.

3) The U-Pb baddeleyite dating results of the gabbros in the Shuikou rock mass show that the crystallization age of the Shuikou rock mass is 210.7 ± 3 Ma (MSWD = 1.01), which belongs to the Late Triassic Indosinian and the peak (258 - 208 Ma) of the strong tensile fracture of the Panxi rift. Based on the comprehensive consideration of geochemical and chronological characteristics, it is believed that the primitive magma of the Shuikou rock mass originated from the low-degree partial melting of the sodic alkali-rich mantle and that the Shuikou rock mass occurred in a continental intraplate tensional environment, which is closely related to the activities of the Emeishan mantle plume during the same period.

Acknowledgements

This study was funded by the Open Fund of State Key Laboratory for Mineral Deposits Research, Nanjing University (No. 2019-LAMD-K12), and a geological survey project (No. DD20211386 and DD20211392) untaken by the Chengdu

Center, China Geological Survey. This study is a collective achievement and we hereby extend our sincere gratitude to all the project team members for their great efforts. Our thanks also go to the reviewers and editors for their valuable suggestions about this manuscript.

Conflicts of Interest

The authors declare no conflicts of interest regarding the publication of this paper.

References

[1] Zhang, Y.X., Luo, Y.N. and Yang, C.X. (1988) Contribution to Panzhihua Xichang Rift. Geological Publishing House, Beijing, 1-325. (In Chinese).

[2] Xu, Y.G. (2000) Distribution of Trace Elements in Spinel and Garnet Peridotites. *Science in China* (*Series D*), **43**, 166-175. https://doi.org/10.1007/BF02878146

[3] Xu, Y.G., Chung, S.L., Jahn, B.M., *et al.* (2001) Petrologic and Geochemical Constraints on the Petrogenesis of Permian-Triassic Emeishan Flood Basalts in Southwestern China. *Lithos*, **58**, 145-168. https://doi.org/10.1016/S0024-4937(01)00055-X

[4] Sterrett, L.E., Ebenroth, E.S., Montgomery, G.S., *et al.* (2011) Pulmonary Limitation to Exercise after Repair of D-Transposition of the Great Vessels: A Trial Baffle versus Arterial Switch. *Pediatric Cardiology*, **32**, 910-916. https://doi.org/10.1007/s00246-011-0013-x

[5] Zhao, Z., Qi, L., Huang, Z.L., Yan, Z.F. and Xu, C. (2010) A Study of Mineralogy and Petrochemistry of Jijie Alkaline-Ultramafic Rocks Southern Part of Panxi Rift. *Earth Science Frontiers*, **17**, 320-335.

[6] Chen, L., Li, J.M., Yang, B., Lü, T. and Li, Z.H. (2013) Distribution of Scandium in the Wujiawan Bauxite Ore-Bearing Rock Series, Southern Chongqing. *Bulletin of Mineralogy, Petrology and Geochemistry*, **32**, 468-474.

[7] Wen, J., Bell, K. and Blenkinsop, J. (1987) Nd and Sr Isotope Systematics of the Oka Complex, Quebec, and Their Bearing on the Evolution of the Sub-Continental Upper Mantle. *Contributions to Mineralogy & Petrology*, **97**, 433-437. https://doi.org/10.1007/BF00375321

[8] Yang, B., Wang, W.Q., Dong, G.C., Guo, Y., Wang, Z.Z. and Hou, L. (2015) Geochemistry, Geochronology and Their Significances of Haizi Bimodal Intrusions in Kangdian Fault-Uplift Zone, Southwestern Margin of Yangtze Platform. *Acta Petrologica Sinica*, **31**, 1361-1373.

[9] Yang, B., Dong, G.C., Guo, Y., Wang, Z.Z. and Wang, P. (2016) Geochemistry, Zircon U-Pb Geochronology and Significances of the Dazhupeng Rhyolites in the Western Yangtze Platform. *Mineralogy and Petrology*, **36**, 82-91.

[10] Huang, X.G., Luo, G.Q. and Li, Y.P. (2016) Study on the Occurrence State of Scandium in Panxi Vanadium-Titanium Magnetite. *Non-Ferrous Metal*, **6**, 1-10.

[11] Xia, B., Liu, H.Y., Zhang, Y.Q., *et al.* (2004) Shrimp Dating of Agpaitic Alkalic Rocks in Panxi Rift Zone and Its Geological Implications—Examples for Hongge, Baima and Jijie Rock Bodies. *Geotectonica et Metallogenia*, No. 2, 149-154.

[12] L, A.R., Smith, M. and Kynicky, J. (2015) From "Strategic" Tungsten to "Green" Neoymium: A Century of Critical Metals at a Glance. *Ore Geology Reviews*, **64**, 455-458. https://doi.org/10.1016/j.oregeorev.2014.06.008

[13] Zhao, Z., Qi, L., Huang, Z.L., Yan, Z.F. and Xu, C. (2012) Trace Elements and Sr-Nd

Isotopic Geochemistry and Genesis of Jijie Alkaline-Ultramafic Rocks, Southern Part of Panxi Rift. *Acta Petrologica Sinica*, **28**, 1915-1927.

[14] Lü, X.J., Cheng, X.X. and Zhou, G.H. (1992) Occurrence State of Scandium in Panzhihua Iron Ore. *Minino and Metallurgical Engineering*, **12**, 35-39.

[15] Le Maitre, R., Bateman, P., Dudek, A., *et al.* (1989) A Classification of Igneous Rocks and Glossary of Terms, Oxford: Subcom Mission on the Systematics of Igneous Rocks. International Union of Geological Sciences, Paris.

[16] MacDonald, G.A. and Katsura, T. (1964) Chemical Compositions of Hawaiian Lavas. *Journal of Petrology*, **5**, 82-133. https://doi.org/10.1093/petrology/5.1.82

[17] Meschede, M. (1986) A Method of Discriminating between Different Types of Mid-Ocean Ridge Basalts and Continental Tholeiites with the Nb-Zr-Y Diagram. *Chemical Geology*, **56**, 207-218. https://doi.org/10.1016/0009-2541(86)90004-5

[18] Zhong, H., Zhu, W.G., Hu, R.Z., *et al.* (2015) Zircon U-Pb Age and Sr-Nd-Hf Isotope Geochemistry of the Panzhihua A-Type Syenitic Intrusion in the Emeishan Large Igneous Province, Southwest China and Implications for Growth of Juvenile Crust. *Lithos*, **110**, 109-128. https://doi.org/10.1016/j.lithos.2008.12.006

[19] Kogiso, T., Hirschmann, M.M. and Pertermann, M. (2004) High-Pressure Partial Melting of Mafic Lithologies in the Mantle. *Journal of Petrology*, **45**, 2407-2422. https://doi.org/10.1093/petrology/egh057

[20] Xia, B., Liu, H.Y. and Zhang, Y.Q. (2007) SHRIMP Dataing of Agpaitic Alkalic Rocks in Panxi Rift Zone and Its Geological Implications: Examples from Hongge, Baima and Jijie Intrusives. *Geotectonica et Metallogenia*, **28**, 149-154.

[21] Wang, C.Y., Zhou, M.F. and Qi, L. (2007) Heterogeneous Mantle Sources and Sulfide Segregation of the Permian Flood Basalts and Mafic Intrusions in the Jin Ping (SW China) and Song Da (Northern Vietnam) District. *Chemical Geology*, **243**, 317-343. https://doi.org/10.1016/j.chemgeo.2007.05.017

[22] Sun, S.S. and McDonough, W.F. (1989) Chemical and Isotopic Systematics of Oceanic Basalts: Implications for Mantle Composition and Processes. In: Saunders, A.D. and Norry, M.J., Eds., *Magmatism in the Ocean Basins*, Special Publication No. 42, Geological Society, London, 313-345. https://doi.org/10.1144/GSL.SP.1989.042.01.19

[23] Sun, S.S. and McDonough, W.F. (1989) Chemical and Isotopic Systematics of Oceanic Basalts: Tectonic Interpretation of Granitic Rocks. *Journal of Petrology*, **25**, 956-983.

[24] Mullen, E. (1983) $MnO/Ti/P_2O_5$: A Minor Element Discriminant for Basaltic Rocks of Oceanic Environments and Its Implications for Petrogenesis. *Earth and Planetary Science Letters*, **62**, 53-62. https://doi.org/10.1016/0012-821X(83)90070-5

[25] Jagoutz, E., *et al.* (1979) The Abundances of Major, Minor and Trace Elements in the Earth's as Derived from Primitive Ultramafic Nodules. *Proceedings of the 10th Lunar and Planetary Science Conference*, Houston, 19-23 March 1979, 2031-2050.

[26] Zou, H., Zindler, A., Xu, X., *et al.* (2000) Major, Trace Element, and Nd, Sr and Pb Isotope Studies of Cenozoic Basalts in SE China: Mantle Sources, Regional Variations, and Tectonic Significance. *Chemical Geology*, **171**, 33-47. https://doi.org/10.1016/S0009-2541(00)00243-6

[27] Zhao, Z., Qi, L., Huang, Z.L. and Xu, C. (2009) The Analytical Methods for Determination of Platinum Group Elements in Geological Samples. *Earth Science Frontiers*, **16**, 181-193.

[28] Zhao, Z., Qi, L., Huang, Z.L., Yan, Z.F. and Xu, C. (2010) The Geochemical Cha-

racteristics of Platinum-Group Elements of Jijie Alkaline-Ultramafic Rocks, Yunnan Province. *Acta Petrologica Sinica*, **26**, 938-946.

[29] Bedard, J.H. (2005) Partitioning Coefficients between Olivine and Silicate Melts. *Lithos*, **83**, 394-419. https://doi.org/10.1016/j.lithos.2005.03.011

[30] Bedard, J.H. (2007) Trace Element Partitioning Coefficients between Silicate Melts and Orthopyroxene: Parameterizations of D Variations. *Chemical Geology*, **244**, 263-303. https://doi.org/10.1016/j.chemgeo.2007.06.019

[31] Bedard, J.H. (2014) Parameterizations of Calcic Clinopyroxene—Melt Trace Element Partition Coefficients. *Geochemistry*, *Geophysics*, *Geosystems*, **15**, 303-336. https://doi.org/10.1002/2013GC005112

[32] Chassé, M., Griffin, W.L., O'Reilly, S.Y. and Calas, G. (2016) Scandium Speciation in a World-Class Lateritic Deposit. *Geochemical Perspectives Letters*, **3**, 105-114. https://doi.org/10.7185/geochemlet.1711

[33] Chassé, M., Griffin, W.L., O'Reilly, S.Y. and Georges, G. (2018) Insights into the Mantle Geochemistry of Scandium from a Meta-Analysis of Garnet Data. *Lithos*, **310**, 409-421. https://doi.org/10.1016/j.lithos.2018.03.026

[34] Williams-Jones, A.E. and Migdisov, A.A. (2014) Experimental Constraints on the Transport and Deposition of Metals in Ore-Forming Hydrothermal Systems. In: Kelley, K.D. and Golden, H.C., Eds., *Building Exploration Capability for the* 21*st Century*, Vol. 18, Society of Economic Geologists, Littleton, 77-95. https://doi.org/10.5382/SP.18.05

[35] Kalashnikov, A.O., Yakovenchuk, V.N. and Pakhomovsky (2016) Scandium of the Kovdor Baddeleyite-Apatite-Magnetite Deposit (Murmansk Region, Russia): Mineralogy, Spatial Distribution, and Potential Resource. *Ore Geology Reviews*, **72**, 532-537. https://doi.org/10.1016/j.oregeorev.2015.08.017

[36] Rudnick, R.L. and Gao, S. (2014) Composition of the Continental Crust. In: Holland, H.D. and Turekian, K.K., Eds., *Treatise on Geochemistry*, Elsevier, Oxford, 1-51. https://doi.org/10.1016/B978-0-08-095975-7.00301-6

[37] Altinsel, Y., Topkaya, Y., Kaya, Ş. and Şentürk, B. (2018) Light Metals. The Minerals, Metals and Materials Society, Pittsburgh, 1545-1553. https://doi.org/10.1007/978-3-319-72284-9_201

[38] Ahmadnejad F., Zamanian, H. and Taghipour (2017) Mineralogical and Geochemical Evolution of the Bidgol Bauxite Deposit, Zagros Mountain Belt, Iran: Implications for Ore Genesis. Rare Earth Elements Fractionation and Parental Affinity. *Ore Geology Reviews*, **86**, 755-783. https://doi.org/10.1016/j.oregeorev.2017.04.006